Hot Pixel Annealing Behavior in CCDs Irradiated at -84°C

C. J. Marshall, P. W. Marshall, *Member, IEEE*, A. Waczynski, E. J. Polidan, S. D. Johnson,
R.A. Kimble, R.A. Reed, *Member, IEEE*, G. Delo, D. Schlossberg, A.M. Russell, T. Beck, Y. Wen,
J. Yagelowich, and R.J. Hill

Abstract—**A Hubble Space Telescope Wide Field Camera 3 e2v CCD was irradiated while operating at -84 °C and the dark current studied as a function of temperature while the charge coupled device was warmed to a sequence of temperatures up to a maximum of +30°C. The device was then cooled back down to -84° and remeasured. Hot pixel populations were tracked during the warm-up and cool-down. Hot pixel annealing began below -40 °C and the anneal process was largely completed by the time the detector reached +20°C. There was no apparent sharp annealing temperature. Although a large fraction of the hot pixels fell below the threshold to be counted as a hot pixel, they nevertheless sustained a higher leakage rate than the remaining population. The mechanism for hot pixel annealing is not presently understood. Room temperature irradiations do not adequately characterize the hot pixel distributions for cooled applications.**

Index Terms—**radiation effects, CCDs, hot pixels, displacement damage**

I. Introduction

CHARGE coupled devices (CCDs) are currently the preeminent detector in the near ultraviolet (UV) to visible wavelength region for astronomical observations in space and are essential in earth-observing space missions as well. Unfortunately, the performance of CCDs is permanently degraded by total ionizing dose (TID) and displacement damage effects. TID produces threshold voltage shifts on the CCD gates and displacement damage reduces the charge transfer efficiency (CTE), increases the dark current, produces dark current nonuniformities and creates random telegraph noise in individual pixels. In addition to these long term effects, cosmic ray and trapped proton transients also interfere with device operation on orbit. In this paper, we investigate the dark current behavior of CCDs: in particular the formation and annealing of hot pixels. Such pixels degrade the ability of a CCD to perform science and also can present problems to the performance of star tracker functions (especially if their numbers are not correctly anticipated so that the required processing capability to track false stars is not provided).

To date, dark current radiation studies have been performed by irradiating the CCDs at room temperature but this can result in a significantly optimistic picture of the hot pixel count. As illustrated in Fig. 1, we know from the Hubble Space Telescope (HST) that high dark current pixels (so-called hot pixels or dark spikes) accumulate as a function of time on orbit and present a serious problem for some missions [1,2,3].   For example, the HST Advanced Camera for Surveys/Wide Field Camera instrument performs monthly anneals to ambient temperatures (roughly 20°C) despite the loss of observational time, in order anneal partially the ever increasing number of hot pixels. Note that the fact that significant annealing occurs at room temperature is not presently understood since none of the commonly expected defects in Si (e.g. divacancy, E center, and A-center) anneal at such a low temperature. However, previous studies have demonstrated short term annealing effects consistent with the present observations as will be discussed later. For further background about displacement damage in Si see [4] and references therein.

II. The Experiment

The HST Wide Field Camera 3 (WFC3) CCDs are 2048x4096 CCD43s manufactured by e2v with a 15 μm square pixel, a supplemental buried channel, a Multi-Phase Pinned (MPP) implant, and thinning for backside illumination. The device was irradiated at the University of California at Davis cyclotron while operating at -84 °C using a dewar specifically designed for proton irradiations. After the CCD was exposed to <1 x 10^3 cm^{-2} 63 MeV protons for alignment purposes, it was further irradiated in steps to reach cumulative fluences ranging from 8.33 x 10^7 cm^{-2} to 2.50 x 10^9 cm^{-2} which corresponds to 1 month and 30 months, respectively of time in the HST orbit. The correspondence between 63 MeV proton fluence and orbital exposure is based on the equivalence of Non-Ionizing Energy Loss (NIEL) damage rates as predicted for the HST WFC3 environment [5].

Prior to irradiation, a series of baseline measurements (with times appropriate to the temperature) were taken at the CCD's nominal operating temperature of -84°C as well at -40°C, -20°C, -10°C, 0°C, +10°C, +20°C and +30°C with a readout speed of 50 kpixels/s, in MPP mode and at a frame rate of 90 s using both readouts. Our analyses are based on data acquired on half the array from one of these readouts, representing a population of just over 4 million pixels. Note that at -84°C the dark frames required 1.5 hour long integrations in order to gather sufficient signal to resolve accurately leakage current in the presence of read noise of 3 electrons RMS, whereas the exposure time at +30°C was only 10 seconds. This is a result of the exponential dependence of the dark current on temperature. For the long integration measurement, multiple frames were required to allow rejection of transient ionization events resulting from ground level cosmic ray contamination. The CCD was irradiated to 8.33 x 10^7 cm^{-2} at -84°C and the dark current distributions reacquired with multiple 1.5 hour integrations before warming the device. During warm-up, multiple dark frames were remeasured at each of the temperatures cited above. After a 4 hour soak at +30°C, the device was then recooled and measured during the cool down at -40°C and again at -84°C. This entire sequence was repeated twice more to simulate the device response to the proposed annealing schedule after the equivalent of two months and three months of on-orbit proton exposure. Finally, the CCD was exposed to an additional 2.25 x 10^9 cm^{-2} protons to bring the total exposure to the on-orbit equivalent of 30 months, or 2.50 x 10^9 cm^{-2}. At each step, a minimum of three exposures were again acquired to enable rejection of random events such as those due to cosmic rays and proton-induced activation. Random events were defined as signal greater than 40 e$^-$/hr present in one or two, but not three of the exposures.   More details about the experimental set-up and measurement sequence may be found in [6].   Recent measurements following 18 months of annealing at room temperature have been made using exactly the same operating

conditions to characterize further the annealed CCD at temperatures of -84°C as well at -40°C,   -20°C, -10°C, 0°C, +10°C, +20°C and +30°C.

III. Results and Discussion

Fig. 2 shows the comparison of pre versus post exposure dark current distributions after cumulative fluence steps of 1.66 x 10^8 cm^{-2} and 2.5 x 10^9 cm^{-2}. Each data set is based on measurements at -84°C before and after annealing at +30°C. (Note that the pre-irradiation dark current was a Gaussian distribution with a mean of only 0.1 e$^-$/hr and a full width half maximum of ~6 e-/hr.)   Clearly significant annealing is associated with the hot pixels as well as the mean dark current. One of the objectives of this study is to investigate the fate of the pixels that were originally hot pre-anneal, but are apparently no longer hot post-anneal. First we describe the nature of the hot pixels, followed by a description of their annealing characteristics.

A. Description of the Hot Pixels

Following the techniques described in [7] the dark current distribution expected based on the collision kinematics was calculated. It was determined that the "humps" observed on the high dark current sides of the distributions in Fig. 2 are not due to inelastic collisions, and by estimating the maximum expected damage energy and scaling the mean dark current to predict the associated leakage rate [7], it was apparent that the high leakage tail of the distribution (hot pixels) were not caused by large damage events. For our test condition of a 63 MeV proton fluence of 2.5 x 10^9 cm^{-2}, out of over 8 million pixels, the pixels with the largest damage have experienced 6 inelastic collisions, and have damage levels just 12.5 times that of the mean of the distribution. If hot pixels were linearly correlated with deposited damage energy, after annealing, we would expect the highest dark current pixels to have leakage rates of about 24 e-/hr.   This is clearly much less than observed based on Fig. 2.

As has been found by others [e.g. 8, 9, 10], we suspect electric field enhanced emission as the cause of these hot pixels and find that the average activation energy for the hot pixels (e.g. > 40 e$^-$/hr) is only 0.47 eV whereas the "normal" pixels have an average dark current activation energy of ~0.62 eV, in line with [9]. We find that that the Arrhenius plots for the normal pixels are slightly bowed as expected based on work by Widenhorn et al.[11]   They showed that the activation energy for the dark current changes as a function of temperature depending on the relative importance of the diffusion versus depletion dark current. The Arrhenius plots are based on the relation $j_d \propto e^{-E_{act}/kT}$ where j$_d$ is the dark current, E$_{act}$ is the corresponding activation energy, k is the Boltzmann constant and T is the temperature. The hot pixels have activation plots with increased scatter, possibly the result of random telegraph noise which is more likely to occur in high dark current pixels [10]. We attempted to identify breaks in the activation energy plots that would indicate the temperature at which annealing occurred but found that the

scatter in the data, the density of temperatures, and the gradual nature of the annealing process meant there were no obvious break points. In contrast, the mean dark currents were in line with that expected based on the damage factors reported by Srour and Lo. [12].

Finally, we find that the noise in the 'normal' pixels is governed by the read noise (3 e⁻ for these devices) but the noise in the hot pixel populations is in excess of that expected based on Shockley-Read-Hall shot noise as indicated in Fig. 3. This would again argue that the hot pixels are not produced by large inelastic events in a pixel which one would expect to be governed by shot noise. Rather we might suggest that the hot pixels are due to small elastic events which occur in the very small high field regions in the pixel. While we do not have electric field profiles for the devices used in this study, some e2v devices are known to have high field regions that would produce electric field enhanced emission from defects located in the regions [10, 13]. This suggestion is not without precedence. Marshall et al. studied a charge injection device with high field regions and found that the hot pixel introduction rate corresponded with the elastic cross section [7]. Also, Hopkins and Hopkinson [10] found that the occurrence of pixels exhibiting Random Telegraph Signal (RTS) noise scales with the elastic cross section and also that high dark current pixels are most likely to exhibit RTS behavior. This work also based on e2v CCDs. Indeed, increased noise would also be expected since hot pixels are also known to exhibit RTS noise [e.g. 10]. However, the RTS time constants are longer than our measurement times at -84°C [10].

B. Annealing of Hot Pixels

Populations of hot pixels were tracked to identify whether a hot pixel encountered at any step in the above-described measurement sequence is a new hot pixel or an existing one. In all cases, hot pixels were defined as those having greater than 20 electrons per hour for all three reads as well as an average greater than the specified dark current threshold. Fig. 4 shows four distinct hot pixel (>40e⁻/hr) populations at -84°C. The threshold value of >40e⁻/hr is somewhat arbitrary and represents a value of 100 times the mean dark current in the pre-irradiation dark current histogram. With this criterion, we identify hot pixel introduction at a rate of roughly 0.6% of the total population per month equivalent exposure (i.e. 8.33e7 cm⁻²). The figure shows hot pixel populations corresponding to proton exposures representing the first (1 month, R1), second (cumulative 2 month, R2), third (cumulative 3 month, R3) and fourth (cumulative 30 month, R4) exposures. Note that the first month radiation (R1) is an upper limit as the long dark frames were inadvertently contaminated when our ⁵⁵Fe x-ray source used for Charge Transfer Efficiency (CTE) measurement slipped into the dewar far enough to expose the CCD. This problem was corrected immediately and the further data are uncontaminated. We see that in each post irradiation soak at +30°C (anneals A1-A4, respectively) further annealing is observed although the bulk of the annealing is complete after the first soak at +30°C. We find that once a hot pixel anneals, it does not become hot again after further exposures as expected since the probability of a pixel experiencing two damage events is very small. This is also consistent with the generation of hot pixels being a Poisson process, and suggests that all pixels are initially equal without predisposition to becoming hot pixels after irradiation. Note that the presence of random telegraph noise in a small fraction of the hot pixels leads to the observation of pixels that do not appear hot immediately after irradiation but then become hot after the 30°C anneal. The benefit of the 4 hour soaks at +30°C is easily seen in Fig. 4. Although it is difficult to compare differing definitions of hot pixels, the annealing rates for the hot pixels measured here are consistent with those observed on other HST cameras [1,2]. We observe annealing rates between 80% (for the >40e⁻/hr criteria) and 97% (for the >140 e⁻/hr criteria).

As seen in Fig. 5, the growth in the hot pixel population after annealing is linear with fluence. Similar behavior was observed for the other threshold criteria. This is again consistent with the viewpoint of hot pixels as a single event phenomenon governed by random statistics. Previous works [8, 9, 10] indicate that hot pixels are a displacement damage phenomenon, and do not result from ionizing dose, and like the present paper, support the mechanism whereby pixels become hot because they have experienced a displacement damage event occurring in a very small high electric field region of the device.

Fig. 6 shows the number of hot pixels that annealed and had their magnitude fall below 100 x and 200 x the mean of the dark distribution. These levels were chosen because they correspond to the thresholds for the hot pixels identified at -84°C (40e⁻/hr is approximately equal to 100 x the mean dark current immediately after irradiation). Hot pixel populations were tracked during the warm-up and cool-down. It appears that the annealing process starts somewhere below -40°C and continues through warmer temperatures. Note that to the extent that hot pixels have a lower activation energy as observed in [9], we have a built-in source of false positives for annealing as we warm up. That is, as we warm up the dark current increases at different rates for the mean dark current as compared to the hot pixels which tend to have a lower activation energy. For example, $E_{act} = 0.47$ eV corresponds to a higher doubling temperature than the mean pixel at $E_{act} = 0.62$ eV. Hence, as you warm, the mean pixels increase in dark current faster so you call out fewer hot pixels using the 100x and 200x criteria, and this looks like annealing. However, Fig. 6 still shows that there is no sharp temperature at which annealing occurs.

The effort to discern at what temperature annealing begins is hampered by the fact that the pixels have a wide range of activation energies that are themselves changing with temperature. For example, Fig. 7 shows the activation energies of the hot pixels (that successfully annealed) resulting from the 2 month proton exposure as they are

warmed the first time as well as their activation energies measured during their cool-down after the 4 hour soak at +30°C. We see that the initially lowered activation energy typical of that observed for electric field enhanced emission becomes about 0.62 eV after annealing, which is that expected for the normal population of pixels. The annealing rates of hot pixels appears more pronounced than that of the median pixel, and it is not possible to determine from our investigation whether the presence of the high field promotes annealing, or the redistribution of defects, or some other mechanism is involved.

In order to determine the temperature range over which annealing occurred we compare the files at each temperature on the way up, and then the way down from the +30°C soak and from the 18 month room temperature unbiased anneal as well. After the 8.33 x 10^7 cm^{-2} protons fluence, we have a total population of 20,958 pixels that exceeded 80 e$^-$/hr (averaged over three readings, each above 20 e$^-$/hr) at -84°C and of these, 13651 annealed to below 40 e$^-$/hr, again as tested at -84°C. As we warmed, we found that the dynamic range of the test equipment resulted in an increasing number of saturated pixels, even with adjustments made to minimum gain and shortest integration time. Therefore, at each temperature we restrict ourselves further to the subset of pixels that did not saturate before and after the +30°C anneals. For example, we can compare our two -40°C file sets, one on the way up to +30°C and the second on the way back down to -84°C, in order to determine the amount of annealing that occurred above -40°C. The ratio of pixels with thresholds greater than 80 e$^-$/hr before annealing over the same pixels after annealing to < 40 e-/hr are plotted in Fig. 8 at -40°C. The dark current for the bulk of this population of pixels annealed by about a factor of ~2-3 with some pixels showing much larger annealing ratios. The mean dark current at -40°C before the anneal was 130 e$^-$/hr whereas it was only -39 e$^-$/hr after the 30°C anneal. (Note that three quarters of the hot pixels saturate at -40°C and therefore are discarded from the analysis.) There is a small subset of pixels with ratios around one which correspond to pixels that had already annealed before reaching -40°C during the first warm-up. This group of pixels is our strongest evidence for annealing below -40°C, however we note that the possibility of random telegraph noise complicates this assessment. Ratios of less than one are present as a result of shot noise and random telegraph noise. Similar results are seen when the histograms of pixels at -20°C, -10°C and 0°C are examined before and after annealing at +30°C, and we see that the annealing has continued up to 0°C. From Table I, we can see that not only is the mean dark current at -20°C, -10°C and 0°C lower after the anneal, but also a substantial proportion of the pixels that were saturated at these temperatures before the anneal were not saturated after the anneal to 30°C, even though identical gain and integration settings were used to make this comparison at a given temperature. Consideration of the reduced number of saturated pixels after the +10°C anneal indicates that

significant annealing continued through +10°C, with little further annealing above +20°C. These results are consistent with the on-orbit experience of the Hubble Space Telescope STIS and ACS instruments.

As seen in Fig. 9, the dark current distributions at -84°C before and after annealing make it clear that the hot pixels anneal much more effectively than the warmer pixels. It is also true that although the annealed hot pixels may have fallen below the threshold to be a hot pixel, they tend not to rejoin the main distribution but rather retain a dark signal that is higher than most other pixels, along with an activation energy which is on average representative of the median pixel at 0.63 eV. Hence we see that although annealing has occurred, stable damage remains.

Finally it is interesting to note that although the dark current annealed significantly on warming from -84°C to +30°C, the charge transfer efficiency, as determined by Fe-55 based CTE measurements at - 84°C before and after annealing, did not anneal, as expected since the defects responsible (primarily the E-center and divacancy) do not anneal until much higher temperatures. It is not currently known what defects and/or device electric fields are responsible for the dark current annealing. However, it is known from the literature that annealing does occur in a variety of Si devices including Si bipolar transistors irradiated at temperatures as low as -60°C [15,16]. Sander and Gregory [15] showed that transient annealing occurred after neutron exposure at -60°C and also at room temperature, and that it was due to the annealing of bulk damage as would be expected in the present case. Srour et al. [16] observed significant short term annealing (from ~2 seconds to ~2 hours) of dark current in n-CCDs following neutron irradiation whereas in contrast, there was negligible annealing of the charge transfer efficiency, consistent with our findings. As in the present case, both Sander et al. and Srour et al. found that stable damage also persisted after the irradiations.

IV. SUMMARY

A HST Wide Field Camera 3 (WFC3) e2v CCD was irradiated with protons while operating at -84 °C and the dark current studied as a function of temperature while the CCD was warmed to a sequence of temperatures up to a maximum of +30°C. The device was then cooled back down to -84° and re-measured. Hot pixel populations were tracked during the warm-up and cool-down. Hot pixel annealing began below -40 °C and the anneal process was largely completed before the detector reached +20°C. The hotter the pixel after irradiation, the more likely it was to anneal. However, there was no sharp annealing temperature. Although a large fraction of the hot pixels fell below the threshold to be counted as a hot pixel, they nevertheless remained warmer than the remaining population. Although the mechanism for dark current annealing is not presently understood, it is consistent with earlier results that exhibit short term annealing after neutron irradiations. Many space applications call for lower temperature operation in order to reduce the dark current, but

it is important to realize also that the number of hot pixels may be increased. During the ground test campaign it must be recognized that room temperature irradiations do not adequately characterize the hot pixel distributions for cooled applications. Further proton energy dependent work would be useful to confirm whether the hot pixel production scales with the elastic cross-section (as reported in [8]) or else the inelastic cross-section as this is important for the prediction of on-orbit behavior. It is also helpful to view the hot pixel problem as a single event phenomenon. As expected, the charge transfer efficiency did not anneal at the temperatures studied.

REFERENCES

[1] M. Sirianni, M. Clampin, G. Hartig, H. Ford, G. Illingworth, V. Argabright, B. Burmester, G. DeMarchi, W. Koldewyn, A. Martel, M. Mutchler, A. Reiss, R. Schrein, and P. Sullivan, "Characterization and on-orbit performance of the Advanced Camera for Surveys CCDs, Proc. SPIE 4854, pp. 496-506, 2003

[2] R. A. Kimble, P. Goudfrootij, and R. L. Gilliland, "Radiation damage effects on the CCD detector of the Space Telescope Imaging Spectrometer," Proc. SPIE 4013, pp. 532-544, 2000.

[3] M. Clampin, G. Hartig, H.C. Ford, M. Sirianni, G. Meurer, A. Martel, J.P. Blakeslee, G.D. Illingworth, J. Krist, R. Gilliland, and R. Bohlin, "Status for the Advanced Camera for Surveys," 2002 HST Calibration Workshop, Space Telescope Science Institute, October 2002.

[4] C. J. Marshall and P. W. Marshall, "Proton effects and test issues for satellite designers, part B: displacement damage effects," 1999 IEEE NSREC Short Course Notes, pp. IV50 – IV110.

[5] C. Dale, P. Marshall, B. Cummings, L. Shamey, and A. Holland, "Displacement damage effects in mixed particle environments for shielded spacecraft CCDs," IEEE Trans. Nucl. Sci., NS-40, pp. 1628-1637, 1993.

[6] E. J. Polidan, A. Waczynski, P. W. Marshall, S. D. Johnson, C. Marshall, R. A. Reed, R. A. Kimble, G. Delo, D. Schlossberg, A. M. Russell, T. Beck, Y. Wen, J. Yagelowich, R. J. Hill, and E. J. Wassell, "Hot pixel behavior in WFC3 CCD detectors irradiated under operational conditions," Proc. SPIE Vol. 5167, pp. 258-269, 2003.

[7] P.W. Marshall, C.J. Dale, and E.A. Burke, "Proton-Induced Displacement Damage Distributions and Extremes in Silicon Microvolumes," IEEE Trans. Nucl. Sci., Vol. 37, No. 6, pp. 1776-1783, 1990.

[8] P.W. Marshall, C.J. Dale, E.A. Burke, G. P. Summers, and G. E. Bender, "Displacement Damage Extremes in Silicon Depletion Regions," IEEE Trans. Nucl. Sci., Vol. 36, No. 6, pp. 1831-1839, 1989.

[9] J.R. Srour and R.A. Hartman, "Enhanced Displacement Damage Effectiveness in Irradiated Silicon Devices," IEEE Trans. Nucl. Sci., Vol. 36, No. 6, pp. 1825-1830, 1989.

[10] I.H. Hopkins and G.R. Hopkinson, "Further Measurements of Random Telegraph Signals in Proton-Irradiated CCDs," IEEE Trans. Nucl. Sci., Vol. 42, No. 6, pp. 2074-2081, 1995

[11] R. Widenhorn, M.M. Blouke, A. Weber, A. Rest, and E. Bodegom, "Temperature dependence of the dark current in a CCD," Proc. SPIE Vol. 4669, pp. 193-201, 2002.

[12] J.R. Srour and D.H. Lo, "Universal Damage Factor for Irradiated-Induced Dark Current in Silicon Devices", IEEE Trans. Nucl. Sci., Vol. 47, No. 6, pp. 2451-2459, 2000.

[13] M. Robbins, "Possibility of Limiting the Radiation Damage Effects in CCDs," HST Detector Workshop, Baltimore MD, January 2000.

[14] E. J. Polidan, A. Waczynski, P. Marshall, S. D. Johnson, C. Marshall, R. Reed, R. A. Kimble, G. Delo, D. Schlossberg, A. M. Russell, T. Beck, Y. Wen, J. Yagelowich, and R. J. Hill, "A Study of hot pixel annealing in the Hubble Space Telescope Wide Field Camera 3 CCDs," Proc. SPIE Vol. 5487, pp. 289-298, 2004.

[15] H. H. Sander and B. L. Gregory, "Transient annealing in semiconductor devices following pulsed neutron irradiation," IEEE Trans. Nucl. Sci., Vol. 13, No. 6, pp. 53-62, 1966.

[16] J. R. Srour, R. A. Hartman, and S. Othmer, "Transient and permanent effects of neutron bombardment on a commercially available n-buried-channel CCD," IEEE Trans. Nucl. Sci., Vol. 27, No. 6, pp. 1402-1410, 1980.
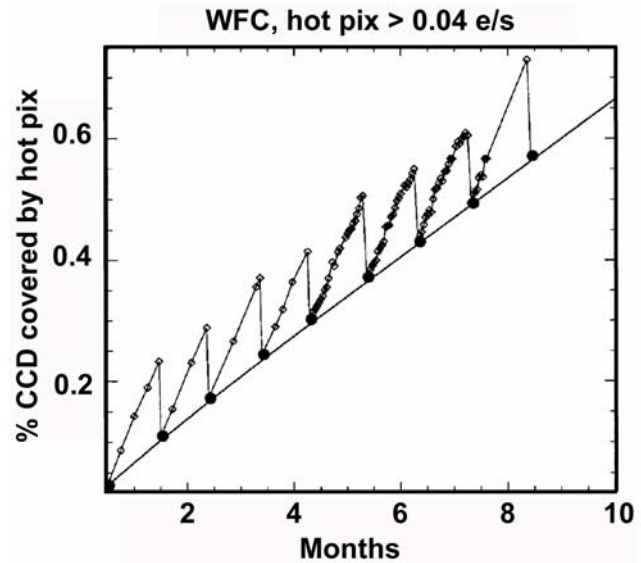
Fig. 1. Hot pixel growth rates require monthly anneals that consume 10% of the observing time on the HST instruments (STIS, WFC2, ACS). From [3].
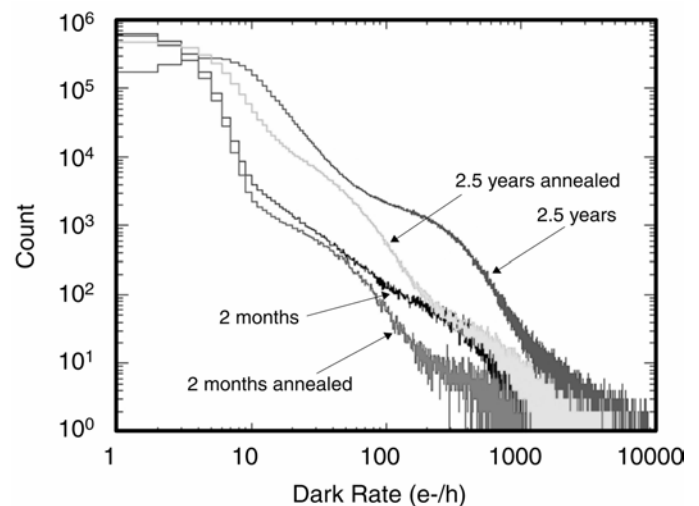

Fig. 2. Comparison of dark current distributions before and after annealing at +30°C for two exposure levels. The data were acquired at -84°C and the pre-irradiation dark current was <0.1 e⁻/hr.
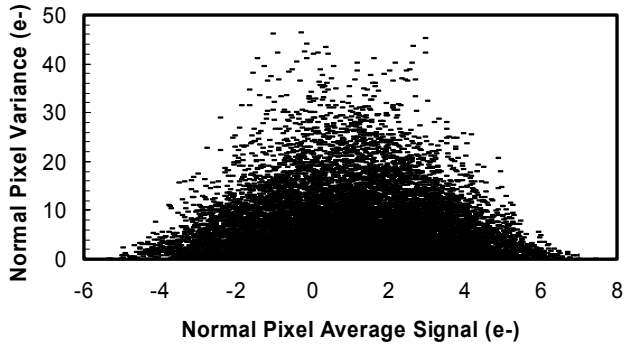
Fig. 4.   Four separate populations of pixels (>40 e⁻/hr) introduced at each radiation step (R1-R4).   In each case, the first anneal is always the most effective at reducing the hot pixel count.

Fig. 3a Scatter plot showing the noise of the normal pixels which is limited by the read noise.

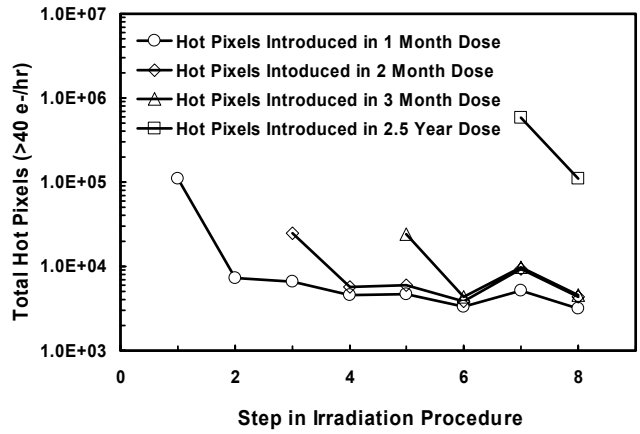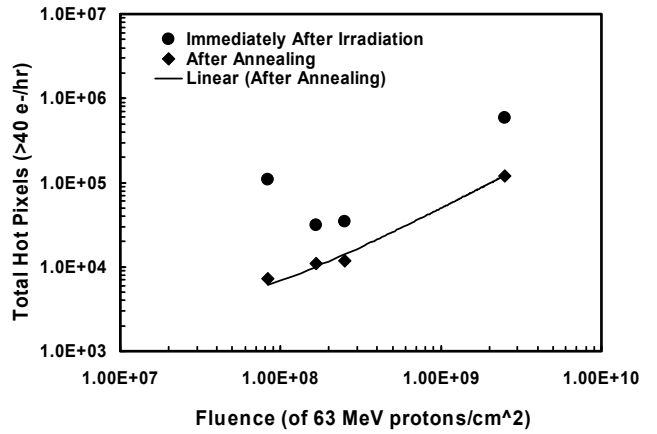Fig. 5 The total number of hot pixels (>40 e⁻/hr) introduced versus proton fluence immediately after irradiation as well as after annealing. The lowest fluence point for the measurements immediately after irradiation is high as a result of the ^{55}Fe source which was inadvertently lowered for this point.

Fig. 3b.   Scatter plot showing the noise in the hot pixels in excess of that expected based on Shockley-Read-Hall shot noise as indicated by the straight line in the figure.
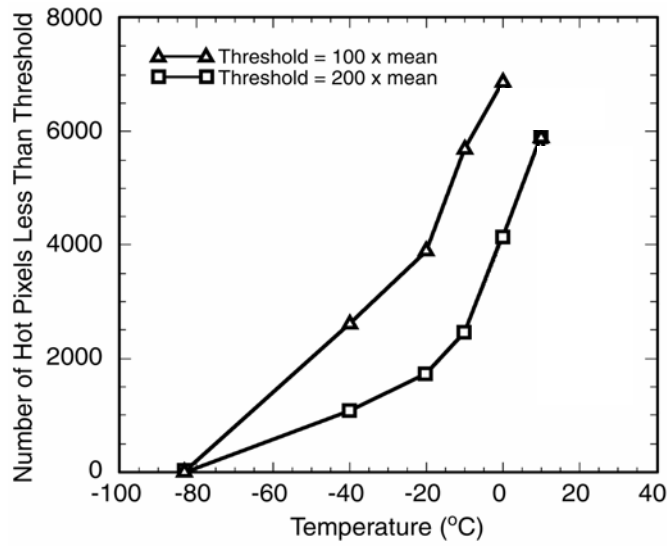
Fig. 6. Number of hot pixels with dark currents below the given thresholds versus temperature. Included are pixels that have annealed as well as some pixels with low activation energies. (Adapted from [14].)
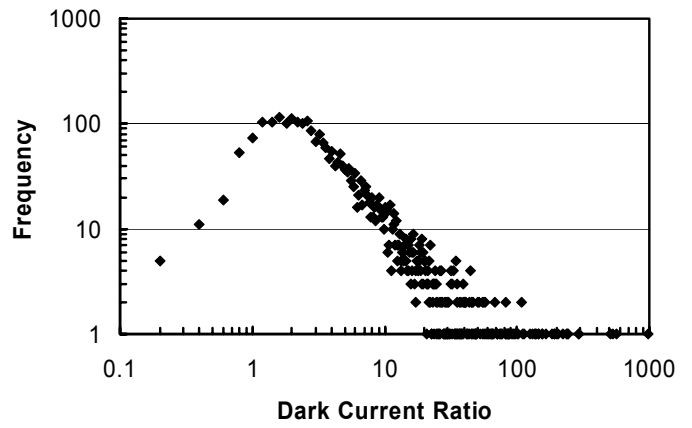

Fig. 8 Histogram of the dark current ratio of annealed hot pixels at -40°C before annealing over the same pixels after annealing to +30°C. Annealed hot pixels are identified as those with dark currents greater than 80 e⁻/hr before annealing that fell below 40 e-/hr after annealing as measured at -84°C.
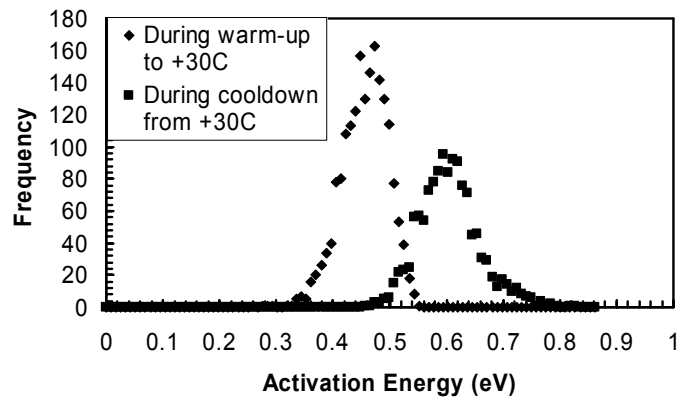

Fig. 7 Histogram of dark current activation energies obtained during the first warm-up after the 2 month proton irradiation, as well as during the cool-down after the 4 hour soak at +30°C. The pixel population includes those hot pixels (>144 e-/hr) that annealed below 40 e-/hr as measured at -84°C after the warm-up to +30°C.
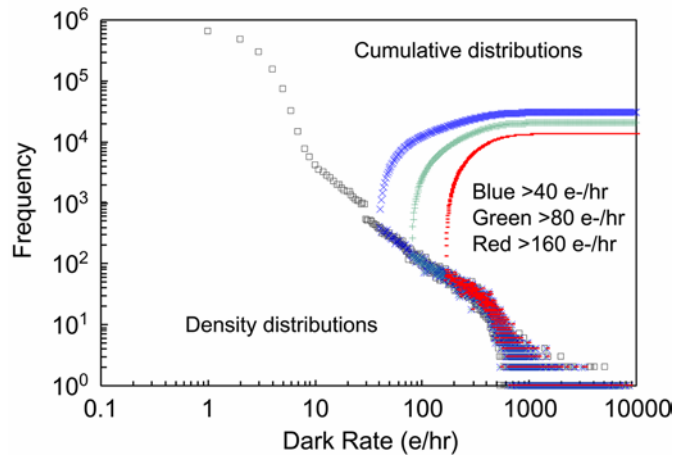

Fig. 9a The distribution of dark signal at -84°C, overplotted with the distributions of the hot pixel populations immediately after irradiation. The upper curves are the corresponding cumulative distributions.
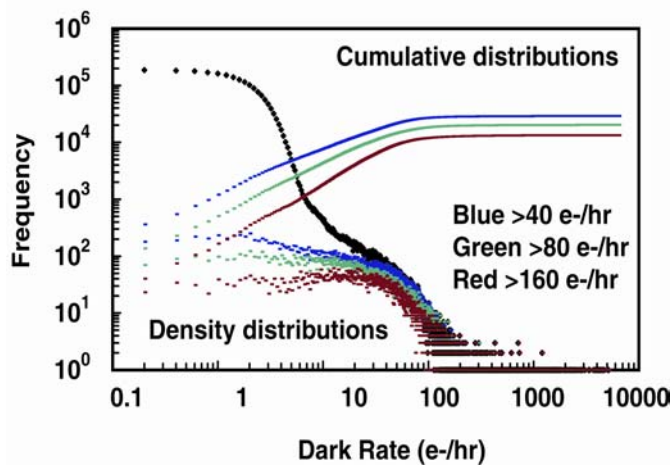.

Fig. 9b. The distribution of dark signal at -84°C, overplotted with the distributions of the hot pixel populations after annealing at +30°C and cooling back to -83°C. The cumulative distributions make it clear that most of the annealed pixels did not return to the main distribution, but rather they are still "warm". For example, for the >40 e⁻/hr group of pixels only 1000 – 2000 out of 20,000 went down to the main part of the distribution

TABLE I
CHARACTERISTICS BEFORE AND AFTER 4 HOUR +30°C ANNEAL

Temp (°C)	A = No. not saturated pixels before anneal	B = No. not saturated pixels after anneal	B/A	C = Mean dark current before anneal (e-/hr)	D = Mean dark current after anneal (e-/hr)	C/D
-40	2781	12946	4.7	3.21e5	1.52e5	2.1
-20	4164	12814	3.1	3.06e5	1.60e5	1.9
-10	9628	13471	1.4	1.33e6	5.53e5	2.4
0	3309	10710	3.2	1.38e6	1.08e6	1.3
10	2824	7662	2.7	1.97e6	2.18e6	0.9
20	1359	1396	1.0	3.08e6	2.09e6	1.1
30	1498	1975	1.3	6.64e6	6.55e6	1.0